Thermal modelling of the ATHENA X-IFU filters

Luisa Sciortino, Ugo Lo Cicero, Salvatore Ferruggia Bonura, Fabio D'Anca, Antonino Buttacavoli, et al.

Luisa Sciortino, Ugo Lo Cicero, Salvatore Ferruggia Bonura, Fabio D'Anca, Antonino Buttacavoli, Elena Puccio, Marco Barbera, "Thermal modelling of the ATHENA X-IFU filters," Proc. SPIE 10699, Space Telescopes and Instrumentation 2018: Ultraviolet to Gamma Ray, 1069950 (6 July 2018); doi: 10.1117/12.2314453

SPIE.

Event: SPIE Astronomical Telescopes + Instrumentation, 2018, Austin, Texas, United States

Thermal Modeling of the ATHENA X-IFU Filters

Luisa Sciortino[*a], Ugo Lo Cicero [b,a], Salvatore Ferruggia Bonura [a,b], Fabio D'Anca [c], Antonino Buttacavoli[b], Elena Puccio[b], and Marco Barbera[a,b]
[a]Università degli Studi di Palermo - Dipartimento di Fisica e Chimica (UNIPA-DiFC), Italy
[b]Istituto Nazionale di Astrofisica - Osservatorio Astronomico di Palermo G.S. Vaiana, Italy
[c] Consiglio Nazionale delle Ricerche - Istituto di BioFisica U.O.S. di Palermo, Italy

ABSTRACT

The X-IFU instrument of the ATHENA mission requires a set of thermal filters to reduce the photon shot noise onto its cryogenic detector and to protect it from molecular contamination. A set of five filters, operating at different nominal temperatures corresponding to the cryostat shield temperatures, is currently baselined. The knowledge of the actual filter temperature profiles is crucial to have a good estimation of the radiative load on the detector. Furthermore, a few filters may need to be warmed-up to remove contaminants and it is necessary to ensure that a threshold temperature is reached throughout the filters surface. For these reasons, it is fundamental to develop a thermal modeling of the full set of filters in a representative configuration. The baseline filter is a polyimide membrane 45 nm thick coated with 30 nm of high-purity aluminum, mechanically supported by a metallic honeycomb mesh. In this paper, we describe the implemented thermal modeling and report the results obtained in different studies: (i) a trade-off analysis on how to reach a minimum target temperature throughout the outer filter, (ii) a thermal analysis when varying the emissivity of the filter surfaces, and (iii) the effect of removing one of the filters.

Keywords: ATHENA, X-IFU, thermal simulation, thermal filters,

1. INTRODUCTION

The X-ray Integral Field Unit (X-IFU), a high spectral resolution energy dispersive detector, is one of the two instruments of the Advanced Telescope for High ENergy Astrophysics (ATHENA) mission. Its array of Transition-Edge Sensor (TES) microcalorimeters will be sensitive in the 0.2-12 keV energy range with an energy resolution of 2.5 eV at 7 keV. Such requirements will exceed the performance of currently operating X-ray observatories like Chandra or XMM-Newton[3].

The X-IFU will operate below 100 mK, requiring a multi stage cryostat to guarantee the requested temperature. The cryostat must have an open optical path to allow the X-rays to reach the detector. However, this path would also let through unwanted radiation (e.g. infrared radiation). A set of filters, named Thermal Filters (TF), are required to attenuate the infrared radiative load on the TES and minimize the energy resolution degradation due to photon shot noise[5].

The TFs shall be both highly transparent in the soft X-ray energy range and reflective in the infrared range, furthermore, they should provide protection from molecular contamination, from low energy particles, and show good mechanical properties. The baseline design of the TFs is based on experience from previous missions such as Chandra and XMM-Newton [7][8][8], since the filters of such astrophysical observatories are still working with no signs of degradation [10][10]. According to the current design the filters will be made of a thin film of aluminized polyimide to achieve both high X-ray transmission and good infrared reflection. On the other hand, the thermal conductance of thin films is very poor, so the filters would not reach the temperature of their corresponding shields. However, the presence of a metallic mesh, the role of which is to give mechanical support to the filter, provides a more efficient thermalization of the TFs. Here, we report stationary computational studies of the TFs thermal behavior in different configurations.

[*] Corresponding author: luisa.sciortino@unipa.it

Space Telescopes and Instrumentation 2018: Ultraviolet to Gamma Ray, edited by Jan-Willem A. den Herder, Shouleh Nikzad, Kazuhiro Nakazawa, Proc. of SPIE Vol. 10699, 1069950 · © 2018 SPIE
CCC code: 0277-786X/18/$18 · doi: 10.1117/12.2314453

2. CURRENT DESIGN AND THERMAL MODELING INPUT PARAMETERS

2.1 Current design of thermal filters

The two filters closer to the detector are mounted on the focal plane assembly, the outer three are fixed to the dewar shells, which are part of the cryogenic cooling system. Each filter consists of a thin polyimide membrane (45 nm thick) coated with an aluminum film (~30 nm thick). They are named using the acronym TF followed by the value of their nominal shield temperature in Kelvin, namely: 200, 100 and 30 for the dewar filters, 2 and 0 (for simplicity instead of 0.05) for the focal plane ones. The only interaction between the filters is by radiative transfer, since they are in direct contact only with their corresponding shields and the instrument operates under vacuum. A clarifying schematic of the filter stack is reported in figure 1, and geometrical parameters are reported in table 1.

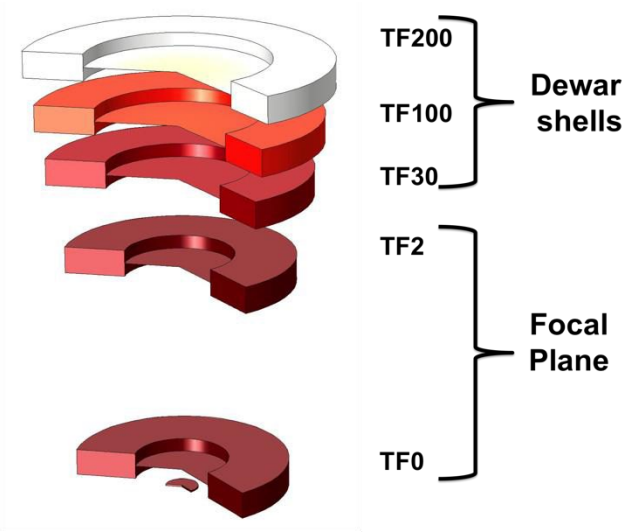

Figure 1. Geometric model of the currently investigated thermal filters assembly.

Table 1. Geometrical parameters of the thermal filters used in the model. T is the nominal filter temperature, corresponding to the shield temperature, Z is the distance from the detector, and D is the filter diameter.

Filter Name	T (K) Shield temperature	Z (mm) Distance from detector	D (mm) Diameter of the filter
TF200	200	240	100
TF100	100	210	88
TF30	30	180	76
TF2	2	130	56
TF0	0.05	15	26

To provide mechanical strength and radio frequency attenuation, a metallic mesh is required. Different materials for the meshes are under evaluation; niobium is being considered for the TF0 mesh, stainless steel (SS) 304 plated with at least 5 μm of gold for the other four filters. The geometrical parameters of the currently evaluated hexagonal meshes are reported in table 2.

Table 2. Geometrical parameters of the currently evaluated hexagonal meshes.

Filter	Mesh pitch (mm)	Mesh material	Wire thickness (µm)	Wire width (µm)	Plating thickness (µm)	BF (%)
TF200	5	SS/Ag	80	40	10	2.4
TF100	5	SS/Au	80	40	5	2.0
TF30	5	SS/Au	80	40	5	2.0
TF2	2	SS/Au	40	20	5	3.0
TF0	2	Nb	40	20	-	2.0

As described, the meshes of TF200, TF100, TF30, and TF2 are composed by a combination of two different materials. A sketched section of a mesh wire is depicted in figure 2 as example.

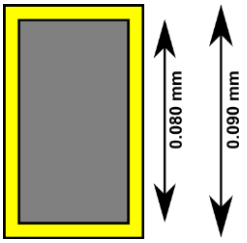

Figure 2. Section of a TF100 and TF30 mesh wire. In grey the SS304 cross-section and in yellow the gold plating one.

The choice of plating the meshes with gold was made to prevent fluorescence emission from the stainless steel wires, induced by background particles. Gold exhibits a higher thermal conductance than the SS304, as a consequence its presence may facilitate the thermalization of the TFs.

2.2 Material properties

Temperature dependent thermal conductivity, k, is considered in the modeling. The trends of k for gold[12] and SS304[13] are plotted in figure 3.

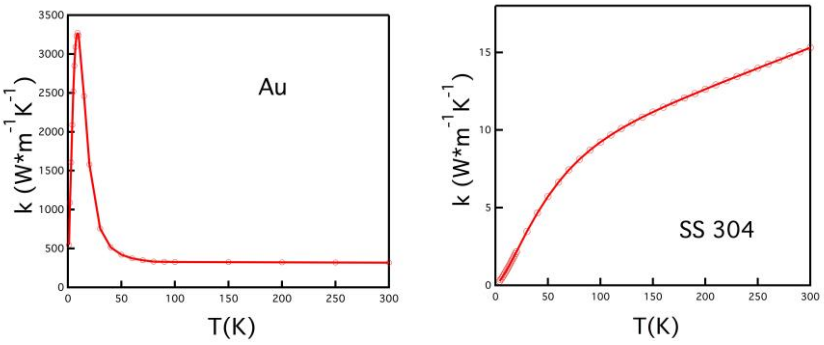

Figure 3. Thermal conductivity of gold (left panel) and SS304 (right panel) as a function of temperature.

The thermal conductivity of gold is hundreds of times higher than that of SS304. Each mesh is modeled with a single equivalent material; for TF30, TF100 and TF200, the mesh thermal conductivity k_{mesh} is obtained by weighting the SS304 and gold conductivities with their cross sections, as illustrated in figure 2. k_{mesh} is therefore calculated as follows:

$$k_{mesh}(T) = k_{SS}(T) \cdot A_{SS} + k_{Au}(T) \cdot A_{Au}, \qquad (1)$$

where k_{SS} and k_{Au} are the thermal conductivities of SS304 and gold respectively, while A_{SS} and A_{Au} are the fractional cross section areas of SS304 and gold. A_{SS} and A_{Au} values are summarized in table 3 for different mesh configurations.

Table 3. Gold and SS304 fractional cross section areas for different mesh configurations.

Wire thickness (µm)	Wire width (µm)	Plating thickness (µm)	A_{SS}	A_{Au}
80	40	10	0.533	0.467
80	40	5	0.711	0.289
40	20	5	0.533	0.467

The TF0 mesh is made of pure niobium, which at 50 mK is known to be in superconducting state[15].; since at such low temperatures the actual thermal properties are strongly dependent on included impurities and on the material processing, measurements on the specific material to be used will be needed. Because of the lack of information, data for the TF0 is not reported in this paper.

To simplify the model, we replaced each mesh with a uniform layer with the same thermal conductivity and an equivalent thickness. This thickness is calculated as the mesh thickness multiplied by the blocking factor that is the ratio between the area covered by the mesh and the filter area.

3. PRELIMINARY ASSESSMENT

The emissivity of aluminum [16] is well known to be very low (~0.05), on the contrary the emissivity of bulk polyimide may have quite high values. However, the emessivity is a surface property, valid generally for opaque bodies. Its use can be extended for computation to semi-transparent thin bodies, but the equivalent emissivity has to be considered as a function of temperature and film thickness [17] Moreover, in our case, the aluminum coating on the opposite face will influence the equivalent emissivity of the polymide face. At the thermal equilibrium

$$t + r + e = 1 \qquad (2)$$

Where, τ is the transmissivity, ρ is the reflectivity, and ε is the emissivity.

Infrared (IR) transmission spectra for polyimide, reported in [18] show variations in relation to the temperature. This effect might be explained with an increase of the reflectivity/emissivity with decreasing temperatures. In a conservative hypothesis we can assume that the reflectivity is unchanged while the emissivity increases cooling down the polyimide. From those data we can conclude that the emissivity of the polyimide is at most 0.04 at 300 K, and 0.06 at 50 K. Because of limitations of the simulation software, we are only inlcuding in the computation the emitted and the reflected components neglecting the transmitted one. Anyway, from [18] it is clear that the IR transmission of 30 nm of Al in the range 1-10 µm is 10^{-2}-10^{-4}, and we can safely assume that the main components are the emitted and the reflected.

The TF200 Al side faces the telescope, that will be kept at 300 K in flight [19]. For all the filters the Al side is directed toward the stages at higher temperature and the polyimide side toward the colder stages.
Between two consecutive filters, each TF is protected laterally from additional heat load by a baffle at the same temperature of the colder shield. We also assume that the emissivity of the upper and the lower surfaces of the TFs frames are different. Lower surfaces shall be shiny, with a low emissivity (0.05). Upper surfaces shall be made as close as possible to a black body, and we assume that their emissivity is 1.

3.1 Temperature profile inside a single element of a mesh

In order to verify the validity of our approximation of substituting the mesh with a homogeneous film, as described in the last paragraph of section 2.2, the thermal gradient inside a single element of a mesh (cell) was simulated as a function of polyimide emissivity (0.05, 0.15, 0.5, 1).

The simulations were carried out using a 2D model, schematically depicted in figure 4. The reported case is referred to the TF100, and the input parameters are: mesh pitch 5 mm, polyimide thickness 45 nm, Al thickness 30 nm, and aluminum emissivity equal to 0.05. The temperature in the contact region between the mesh (fig.4 in grey) and the polyimide (fig.4 in red) is fixed at 100 K. For the simulation showed in this paragraph the ambient temperatures are 300 K, for the aluminum side, and 100 K, for the polymer side.

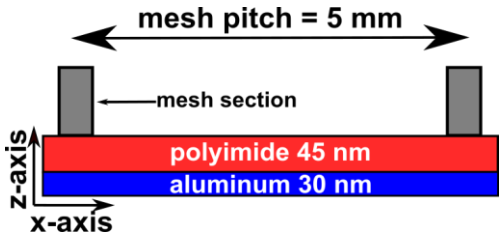

Figure 4. Section of a single element of the TF100 used for the study of the temperature profile inside the single element. In gray the section of the mesh, in red the polyimide, and in blue the aluminum.

The thermal conductivity of polyimide and aluminum are set to 0.149 $Wm^{-1}K^{-1}$ [14] and 3000 $Wm^{-1}K^{-1}$ [20], respectively. In such conditions, we evaluate the temperature profiles along both the *x* and *z* axes. The simulated data are reported in figure 5.

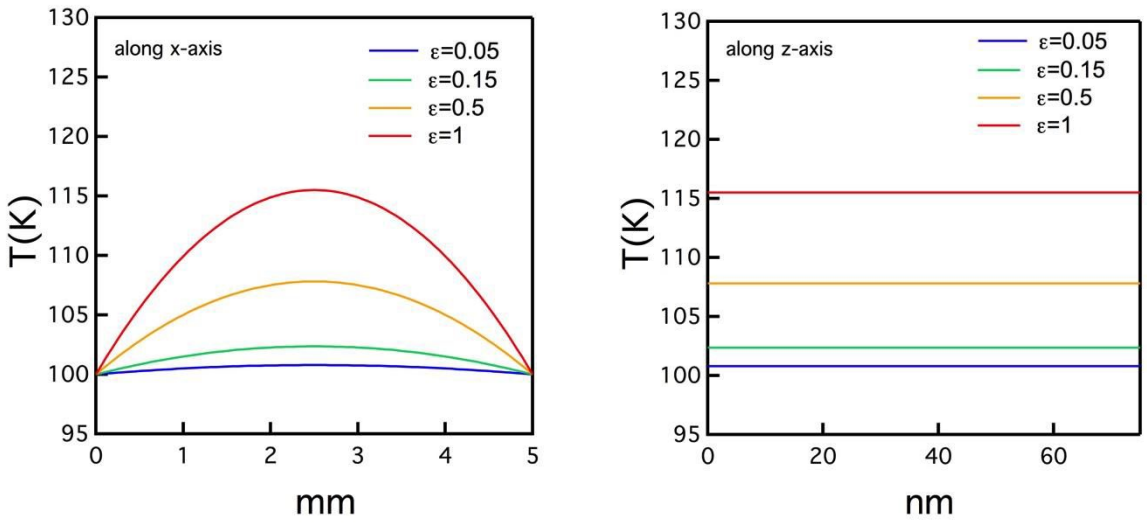

Figure 5. Temperature profiles along one single element of TF100 with mesh pitch of 5 mm. Left panel: Temperature profile along x- direction at different polymer emissivity values 0.05 (blue line), 0.15 (green line), 0.5 (orange line), and 1 (red line). Right panel: Temperature profile along z- direction at different polymer emissivity values 0.05 (blue line), 0.15 (green line), 0.5 (orange line), and 1 (red line).

Along the z-axis the temperature profile is constant for all the considered polyimide emissivities, and we can neglect the temperature gradient across the thickness of the Al and polyimmide films. With regard to the x-axis, the temperature gradient inside a single element of the mesh can be neglected for low values of emissivity. For a smaller pitch the gradient is reduced, because the cell area is lower. The filter at 30 K will show a smaller gradient, since at that temperature the thermal conductivity of aluminum is higher than that at 100 K[13]. Considering that the low emissivity values are the most realistic ones, we can assume that from a thermal point of view each filter can be described as a film composed of the same material of the mesh and thickness such that its mass equals the mesh mass.

3.2 Temperature requirement for the outer filter

One of the tasks that the filters should accomplish is the protection of the detector from molecular contaminants. For previous X-ray missions, such as for the ACIS instrument on Chandra, the molecular contamination of the filters was individuated as one of the crucial causes of the progressive loss of the sensitivity at low energy since the first operating years [21].. The ACIS case suggests the possibility of using a constant or periodic heating to clean the X-IFU filter surfaces from contaminants. Since at 200 K the molecular contamination can already occur, the outer filter, TF200, which is potentially more exposed to contamination, must be kept at temperature higher than the environment. As a consequence, a minimum temperature requirement of 320 K was set for the TF200[21].. A way to meet this requirement would be to heat the frame of the outer filter at higher temperature. A study to determine the needed TF200 frame temperature is carried out and is reported in the next section (section 4.1). In this respect three different options for the TF200 mesh, summarised in table 4, are evaluated and discussed. We evaluate a SS304 mesh coated with 5 μm of gold (option #A), a SS304 mesh coated with 10 μm of gold (option #B), and a SS304 mesh coated with 10 μm of silver (option #C).

Table 4. Mesh materials and thickness of gold (or silver) plating for the three options investigated for the TF200.

OPTION	Mesh material for TF200	Plating thick. (μm)
#A	SS304/Au	5
#B	SS304/Au	10
#C	SS304/Ag	10

4. RESULTS AND DISCUSSION

4.1 Trade-off analysis for heating the outer filter to 320 K

Here, we report the temperature profile of the TF200 at different temperatures of the frame, keeping the emissivity of polyimide at 0.05. The simulation for option #A (left panel of figure 6), a SS304 mesh with 5 μm of gold plating and blocking factor 2%, shows that the frame must be warmed up to 500 K to obtain 320 K at the center of the filter. This is an unfeasible solution for the X-IFU cryostat in terms of thermal budget, so we studied the possibility of a thicker gold plating of the mesh wires to facilitate the thermalization. In option #B we increase the gold plating up to 10 μm, at the expenses of the blocking factor that raises up to 2.4 %. In this case (middle panel of figure 6) the frame must be warmed up to 390 K to obtain 320 K at the center of the filter. In order to decrease further the temperature of the frame we investigate the possibility of use silver instead of gold. Silver has a higher thermal conductivity at 300 K (430 $Wm^{-1}K^{-1}$ [20]) than gold (317 $Wm^{-1}K^{-1}$[14]), and if the thickness is larger than 7 μm it is also efficient in the absorption of fluorescence emissions from the stainless steel wires, as reported in [23].. In this regard the option #C (right panel of figure 6), a SS304 mesh with 10 μm of silver plating, was studied. The temperature profile shows that the frame must be warmed up to 360 K to obtain 320 K at the center of the filter. As a result we can assert that such a configuration might be doable, provided that such frame temperature will be proven compatible with the cryostat thermal budget. This trade-off analysis shows that to warm up the filter at temperature higher than 300 K a thicker plating is necessary both for gold and silver cases, and that silver may be a good solution in terms of efficient thermalization and thermal budget.

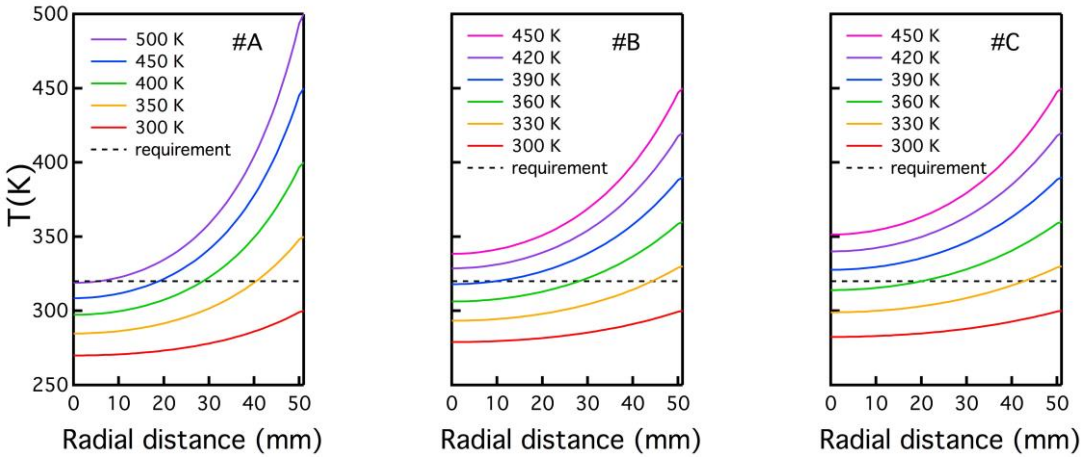

Figure 6. Radial temperature profiles of TF200 with polyimide emissivity set to 0.05. The black dotted line shows the temperature required at the center of the TF200. Left panel: radial temperature profile of TF200 with gold plating thickness 5 μm for frame temperatures of 500 K (purple line), 450 K (blue line), 400 K (green line), 350 K (orange line), and 300 K (red line). Middle panel: radial temperature profile of TF200 with gold plating thickness 10 μm for frame temperatures of 450 K (magenta line), 420 K (purple line), 390 K (blue line), 360 K (green line), 330 K (orange line), and 300 K (red line). Right panel: radial temperature profile of TF200 with silver plating thickness 10 μm for frame temperatures of 450 K (magenta line), 420 K (purple line), 390 K (blue line), 360 K (green line), 330 K (orange line), and 300 K (red line).

4.2 Effects of the polymer emissivity

The thermal behavior of the filters at different values of polymer emissivity was also studied. For all the following reported simulations the input parameters for the TF200 are those of the option #C (see table 2), since silver allows to operate with a colder frame to reach the minimum temperature requirement (see section 4.1). The radial temperature profiles for TF200, TF100, TF30, and TF2 are reported in figure 7 and 8.

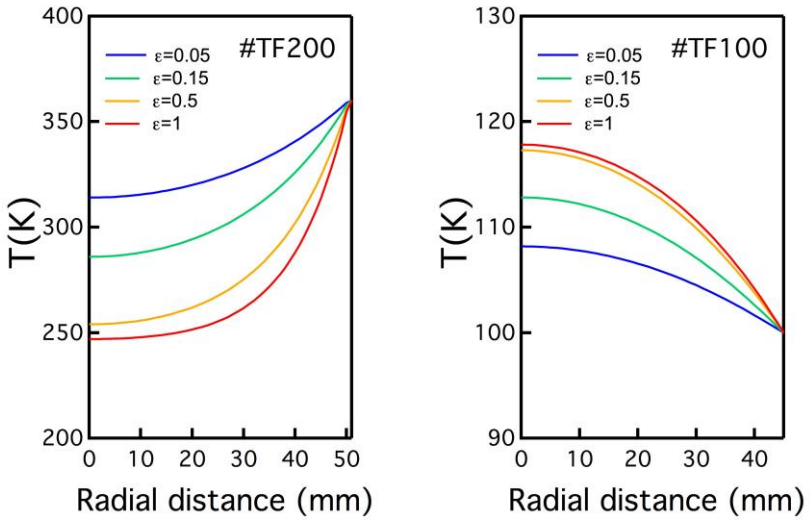

Figure 7. Radial temperature profiles. Left panel, temperature profile of TF200 for different polymer emissivity values: 0.05 (blue line), 0.15 (green line), 0.5 (orange line), and 1 (red line). Right panel, temperature profile of TF100 for different polymer emissivity values: 0.05 (blue line), 0.15 (green line), 0.5 (orange line), and 1 (red line).

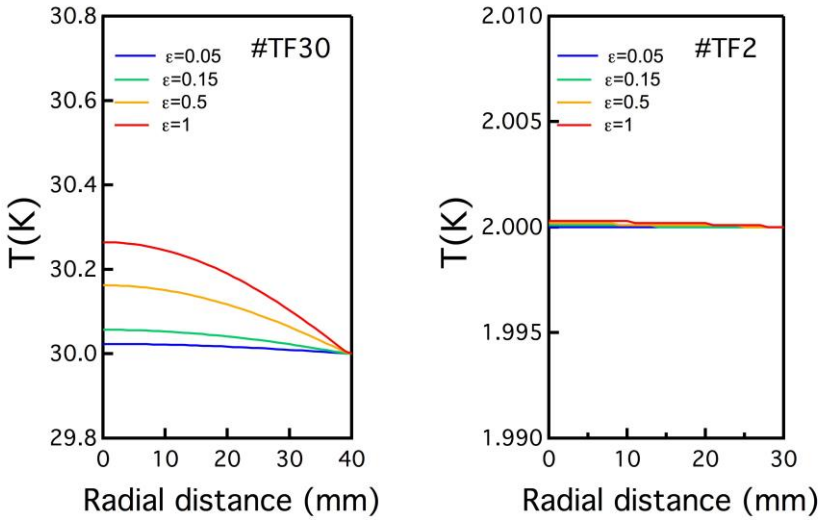

Figure 8. Radial temperature profiles. Left panel, temperature profile of TF30 for different polymer emissivity values: 0.05 (blue line), 0.15 (green line), 0.5 (orange line), and 1 (red line). Right panel, temperature profile of TF2 at different polymer emissivity values: 0.05 (blue line), 0.15 (green line), 0.5 (orange line), and 1 (red line).

The colder filters, TF30 and TF2, have a low sensitivity to the emissivity of the polyimide; on the contrary, TF200 and TF100 are strongly affected by this parameter, even though the effect is completely different in these last two cases. If the emissivity of the TF200 is high, its net radiative emission increases (it is the hottest body in the cryostat) and the filter cools down considerably. On the other hand, the TF100 heats up to 118 K if the emissivity is high, while it warms up to 108 K if the emissivity is 0.05. As a consequence, an experimental campaign to measure the emissivity of 45 nm of aluminized polyimide in the 100-360 K range would be crucial to improve the thermal model of the filters.

4.3 Removal of a filter

In this section, we evaluate the effect of the removal of a filters for two main reasons: to explore the possibility of eliminating one filter in the final design to increase the X-ray transmission, and to analyze the case of a damage that might partially or fully break one of the TFs. Firstly, the occurrence of a localized damage was simulated. Such a damage was supposed to be a hole at the center of one of the filters TF200, TF100, and TF30, with diameter equal to the mesh pitch. In all these cases the presence of a hole does not change the temperature profiles, therefore the resulting numerical data is not reported.

The temperature profiles of TF200, TF100, and TF30 when a filter is removed is reported in figure 9.

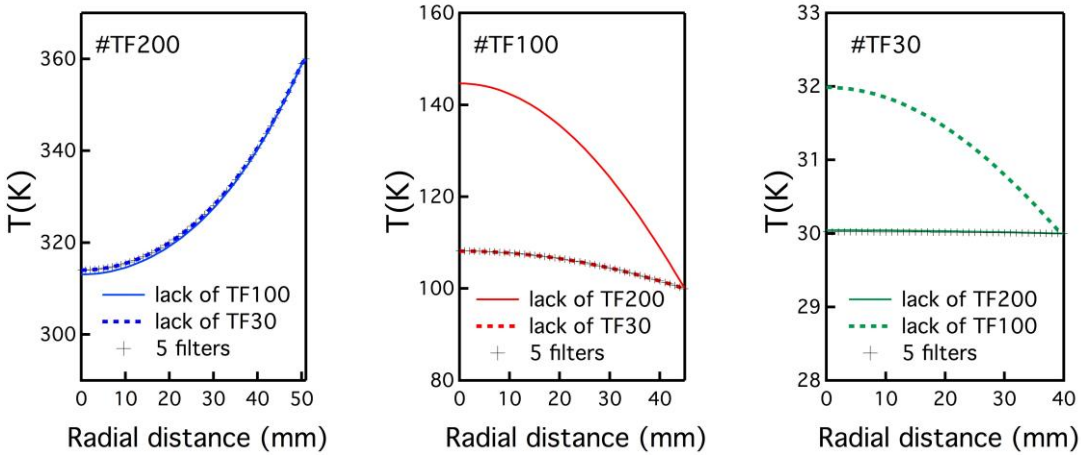

Figure 9. Radial temperature profiles when the removal of a filter occurs. Left panel: temperature profile of TF200 in case of lack of TF100 (blue solid line), lack of TF30 (blue dotted line), and filters all present (black + symbol). Middle

panel: temperature profile of TF100 in case of lack of TF200 (red solid line), lack of TF30 (red dotted line), and filters all present (black + symbol). Right panel: temperature profile of TF30 in case of lack of TF200 (green solid line), lack of TF100 (green dotted line), and filters all present (black + symbol).

The temperature profiles of figure 9 show that TF200 is basically not affected by the removal of TF100 or TF30. On the contrary TF100 is undoubtedly sensible to the absence of the TF200 since the temperature at the center of the filter increases by 36 K, while the lack of TF30 seems not to have any effect on its temperature profile. The TF30 is affected by the removal of TF100 although the increase of the temperature is quite moderate (~2 K).

From these findings, the removal of TF200 is unquestionably unfeasible, on the other hand the removal of TF100 or TF30 might be considered. If the TF100 is removed the effect on the TF200 is negligible and the effect on the TF30 is relatively small, and if the TF30 is removed the effect on both TF200 and TF30 is negligible. Anyway, in these last two cases the evaluation of the photon shot-noise on the detector should be carried out to understand if a configuration with 4 filters might be viable [24].. This solution would increase substantially the X-ray transparency of the filter set, to the advantage of instrument sensitivity.

5. CONCLUSIONS

In conclusion, a simulation based thermal study of the X-IFU TFs is reported. We find that, for the more favorable configuration that envisages a silver plating of 10 μm over the outer filter mesh, the TF200 frame must be warmed at least up to 360 K to obtain 320 K at the center of the filter. The effect of a variation of the polyimide emissivity is also investigated, and our results show that such value affect mainly the two outer filters, and suggest that an experimental campaign to determine the emissivity of 45 nm of aluminized polyimide is essential. Moreover, the removal of a filter (TF200, TF100, and TF30) is studied, and our findings show that is worth to investigate the possibility to reduce the number of filters from 5 to 4, removing the TF100 or the TF30, while the removal of the TF200 is not acceptable.

ACKNOWLEDGMENT

The research leading to these results has received funding from ASI (Italian Space Agency) under the contract n. 2015-046-R.0, from the European Union's Horizon 2020 Program under the AHEAD project (grant agreement n. 654215), and from ESA (European Space Agency) under the contract n. 4000120250/17/NL/BJ. We acknowledge fruitful discussions and support by LUXEL corp.

[1] Barret, D., Trong, T. L., den Herder, J. W., Piro, L., Barcons, X., Huovelin, J., ... & Rauw, G., "The Athena X-ray Integral Field Unit (X-IFU)," Proc. SPIE, Space Telescopes and Instrumentation 2016: Ultraviolet to Gamma Ray, 9905, 99052F, (2016). https://doi.org/10.1117/12.2232432.

[2] Barcons, X., Nandra, K., Barret, D., Den Herder, J.-W., Fabian, A. C., Piro, L., Watson, M. G. and the Athena team, "Athena: the X-ray observatory to study the hot and energetic Universe," J. Phys.: Conf. Ser. 610, 012008, 1-8 (2015). https://doi.org/10.1088/1742-6596/610/1/012008.

[3] Weisskopf, M.C., Tananbaum, H.D., Van Speybroeck, L.P., O'Dell, S.L. "Chandra X-ray Observatory (CXO): overview", Proc. SPIE 4012, X-Ray Optics, Instruments, and Missions III, (18 July 2000); https://doi.org/10.1117/12.391545F.

[4] Jansen, D. Lumb, B. Altieri, J. Clavel, M. Ehle, C. Erd, C. Gabriel, M. Guainazzi, P. Gondoin, R. Much, R. Munoz, M. Santos, N. Schartel, D. Texier, G. Vacanti Astron. Astrophys. 365, L1–L6, (2001) https://doi.org/10.1051/0004-6361:20000036.

[5] Charles, I., Daniel, C., André, J., Duband, L., Duval, J-M., den Hartog, R., Mitsuda, K., Shinozaki, K., van Weers, H., Yamasaki, N.Y. "Preliminary thermal architecture of the X-IFU instrument dewar", Proc. SPIE 9905, Space Telescopes and Instrumentation 2016: Ultraviolet to Gamma Ray, 99052J (18 July 2016); https://doi.org/10.1117/12.2232710.

[6] Barbera, M., Argan, A., Bozzo, E. et al. J. Low Temp. Phys.184: 706 (2016) https://doi.org/10.1007/s10909-016-1501-4.

[7] Barbera, M., Austin, K., Collura, A., Flanagan, A., Jelinsky, R., Murray, S., Serio, S., Zombeck, M., "Development of the UV/ion shields for the Advanced X-ray Astrophysics Facility high-resolution camera (AXAF HRC)", Proc. SPIE 2280, EUV, X-Ray, and Gamma-Ray Instrumentation for Astronomy V, (16 September 1994); https://doi.org/10.1117/12.186815.
[8] Meehan, R., Murray. S., Zombeck, V., Kraft, P., Kobayashi, K., Chappell, H., Kenter, T., Barbera, M., Collura, A., Serio, S., "Calibration of the UV/ion shields for the AXAF High-Resolution Camera", Proc. SPIE 3114, EUV, X-Ray, and Gamma-Ray Instrumentation for Astronomy VIII, (15 October 1997); https://doi.org/10.1117/12.283790.
[9] Villa, G.E., Barbera, M., Collura, A., La Palombara, N., Musso, C., Serio, S., Stillwell, R., Tognon, P., Turner, D.C., "The optical/UV filters for the EPIC experiment." Nuclear Science Symposium, 1997. IEEE 1 (1997). doi: 10.1109/NSSMIC.1997.672658.
[10] Barbera, M., Agnello, S., Buscarino, G., Collura, A., Gastaldello, F., La Palombara, N., Lo Cicero, U., Tiengo, A., Sciortino, L., Varisco, S., Venezia, A.M., "Status of the EPIC thin and medium filters on-board XMM-Newton after more than 10 years of operation: 1) laboratory measurements on back-up filters", Proc. SPIE 8859, UV, X-Ray, and Gamma-Ray Space Instrumentation for Astronomy XVIII, 885914 (26 September 2013); https://doi.org/10.1117/12.2030896.
[11] Gastaldello, F., Barbera, M., Collura, A., La Palombara, N., Lo Cicero, U., Sartore, N., Tiengo, A., Varisco, S., "Status of the EPIC thin and medium filters on-board XMM-Newton after more than 10 years of operation: 2) analysis of in-flight data", Proc. SPIE 8859, UV, X-Ray, and Gamma-Ray Space Instrumentation for Astronomy XVIII, 885915 (26 September 2013); https://doi.org/10.1117/12.2030897.
[12] http://www.efunda.com/materials/elements/TC_Table.cfm?Element_ID=Au
[13] http://www.efunda.com/materials/elements/TC_Table.cfm?Element_ID=Al
[14] https://trc.nist.gov/cryogenics/materials/materialproperties.htm LNG Materials and Fluids. Ed. Douglas Mann National Bureau of Standards, Cryogenics Division First Edition, 1977.
[15] Finnemore, D.K., Stromberg, T.F., & Swenson, C.A. "Superconducting properties of high-purity niobium." Phys. Rev., 149, 231 (1966); https://doi.org/10.1103/PhysRev.149.231.
[16] Giulietti, D., Lucchesi, M., "Emissivity and absorptivity measurements on some high-purity metals at low temperatures." Journal of Physics D: Applied Physics, 14, 877 (1981); https://doi.org/10.1088/0022-3727/14/5/019.
[17] Gardon, R. "The emissivity of transparent materials." Journal of the American Ceramic Society, 39, 278-285 (1956); https://doi.org/10.1111/j.1151-2916.1956.tb15833.x.
[18] Barbera, M., Lo Cicero, U., Sciortino, L., Magnano, E., Píš, I., Ciaravella, A., Collura, A., Jimenez Escobar, A., Levantino, M., Nuzzo, F.,"Temperature effects on the performances of the ATHENA X-IFU thermal filters.", Proc. SPIE 9905, Space Telescopes and Instrumentation 2016: Ultraviolet to Gamma Ray, 990560 (18 July 2016); https://doi.org/10.1117/12.2232323.
[19] Ayre, M., Bavdaz, M., Ferreira, I., Wille, E., Fransen, S., Stefanescu, A., & Linder, M.,"ATHENA: system studies and optics accommodation.", Proc. SPIE 9905, Space Telescopes and Instrumentation 2016: Ultraviolet to Gamma Ray, 990526 (18 July 2016); https://doi.org/10.1117/12.2234275.
[20] Powell, R. W., Ho, C. Y., & Liley, P. E. [Thermal conductivity of selected materials] Washington, D. C: US Government Printing Office, (1966).
[21] Plucinsky, P.P., Bogdan, A., Germain, G., & Marshall, H. L. "The evolution of the ACIS contamination layer over the 16-year mission of the Chandra X-ray Observatory." Proc. SPIE 9905, Space Telescopes and Instrumentation 2016: Ultraviolet to Gamma Ray, 990544 (18 July 2016); https://doi.org/10.1117/12.2233837.
[22] "X-IFU Optical Thermal blocking Filter requirements document", XIFU-RD-10000-00347-CNES (Private communication – draft).
[23] Perinati, E., Barbera, M., Diebold, S., Guzman, A., Santangelo, A., & Tenzer, C. "Preliminary assessment of the ATHENA/WFI non-X-ray background." Exp. Astr., 44, 387-399 (2017).
[24] M. Barbera, et al., "Athena X-IFU thermal filters development status towards the end of the instrument phase-A", these proceedings (2018).